Isotope effects on antiproton and muon capture by hydrogen and deuterium atoms and molecules

James S. Cohen*

Theoretical Division, Los Alamos National Laboratory, Los Alamos, New Mexico 87545
(Received 24 August 1998)

Cross sections for capture of the antiproton ($\bar{p}$) and negative muon (μ^-) by the H_2 and D_2 molecules are calculated using fermion molecular dynamics (FMD). All the cross sections are significantly larger than those for capture by the corresponding atom, also evaluated by the FMD method. The largest molecular cross sections are obtained when the negative projectile mass best matches the nuclear mass in the molecular target, thus for $\bar{p} + H_2$. The vibrational degree of freedom is shown to be most important in distinguishing the four reactions, but the effects of rotations, two-center electronic charge distribution, and nonadiabaticity are also significant. The predicted *initial* capture fractions (i.e., not taking subsequent transfer into account) in a $H_2 + D_2$ mixture are $P_{\text{capt}}^{(p)}/P_{\text{capt}}^{(d)} = q c_p / c_d$, where $q = 1.585$ for $\bar{p}$ and $q = 1.186$ for μ^- independent of c_p and c_d. The energy-dependent quantum-number distributions of the exotic atoms formed, the angular distributions of antiprotonic atoms, and the initial kinetic energies of muonic atoms are also presented.
[S1050-2947(99)06602-0]

PACS number(s): 36.10.−k, 34.10.+x, 25.43.+t, 03.65.Sq

I. INTRODUCTION

Recently a method was implemented that is able to take into account the effect of molecular degrees of freedom on heavy negative-particle capture [1]. Rotations and especially vibrations were found to dramatically enhance antiproton capture by the hydrogen molecule over that by the hydrogen atom. Analysis of the various motions showed that the enhancement comes from efficient energy transfer from the antiproton projectile to the equal-mass proton nucleus in the H_2 target. Thus it may be expected that capture will be optimum where the mass of the negative projectile matches that of an atom in the target molecule and that the molecular enhancement will diminish as the mass match deteriorates.

In the present work, calculations are performed for capture of antiprotons ($\bar{p}$, of mass $1836.15 m_e$) and negative muons (μ^-, of mass $206.77 m_e$) by H_2 and D_2, which have projectile-to-target-nucleus ratios 1.00, 0.50, 0.113, and 0.056. Before the work of paper I it had been generally thought that negative-particle capture was almost entirely due to *quasiadiabatic ionization* [2], in which case the captures of $\bar{p}$ and μ^- by atomic hydrogen or various isotopes of molecular hydrogen would all be expected to be essentially the same in their respective center-of-mass systems (of course, *kinematic* differences occur in the laboratory system). Based on the new understanding, such similarity could no longer be expected, but it remained to be seen how influential the internal molecular degrees of freedom would still be for a considerably poorer mass match like $\mu^- + D_2$. The present work answers this question.

Antiproton and negative muon capture have long been of interest, but the connection of theory with experiment has generally been made via stopping ranges, which do not depend much on the final collision in which capture occurs, and

via the quantum numbers of the initial capture orbital, which is related to observed x rays only after a rather complicated cascade. This situation is about to be dramatically improved for antiproton capture. An experiment [3], scheduled at the forthcoming antiproton decelerator (AD) at CERN, will measure the antiproton capture cross section for H_2 and D_2 at specifiable incident antiproton energies.

The theoretical approach described in Sec. II is the same as that in paper I. The method is termed fermion molecular dynamics (FMD), though it has also sometimes been denoted after its developers as ''KWC'' (Kirschbaum-Wilets-Cohen), or as quasiclassical-trajectory Monte Carlo (QTMC) in analogy to the widely used classical-trajectory Monte Carlo (CTMC) method. In the case of one-electron atomic targets, the FMD method is similar to the CTMC method except that it takes some quantum-mechanical effects into account. For μ^- capture by the hydrogen atom the FMD method has been shown [4] to produce even better agreement with the benchmark classical-quantal coupling (CQC) calculation [5] than did the CTMC method [6]. Unlike the CTMC method, FMD is also applicable to multielectron systems. Paper I showed how the Kirschbaum-Wilets (KW) ansatz [7] could be extended for an accurate description of the H_2 and H_2^+ molecules.

In Sec. III the FMD formulation is used to perform full five-body dynamics on the systems $\bar{p} + H_2$, $\bar{p} + D_2$, $\mu^- + H_2$, and $\mu^- + D_2$. The capture cross sections and quantum numbers of the exotic atoms formed are compared with each other and with results for the analogous atomic targets.

II. THEORETICAL METHOD

A. Effective Hamiltonian

The effective Hamiltonian is written

$$H_{\text{KWC}} = H_0 + V_{\text{pseudo}}, \qquad (1)$$

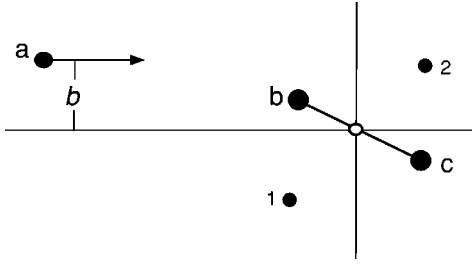---

*Electronic address: cohen@lanl.gov

FIG. 1. Particle labeling: a = incident $\bar{p}$ or μ^- with impact parameter b, b and c=nuclei p or d of H_2 or D_2 target, 1 and 2= electrons of target molecule, o=geometric center of molecule.

where

$$H_0 = T + V_{\mathrm{Coul}} \tag{2}$$

is the usual Hamiltonian containing the kinetic energy and Coulomb potentials and

$$V_{\mathrm{pseudo}} = V_H + V_P + V_{m1} + V_{m2} \tag{3}$$

is a sum of repulsive pseudopotentials that tend to preclude the system from quantum mechanically forbidden regions of phase space (tunneling into nonclassical regions is not taken into account).

The term V_H serves to prevent collapse of an electron to a nucleus; quantum mechanically this can be thought of as a consequence of the Heisenberg uncertainty principle and the KW implementation is equivalent to the Bohr–de Broglie quantization condition [8]. The term V_P provides an additional repulsion between two electrons having the same spin, which is the quantum-mechanical effect of wave-function antisymmetry. These two terms serve to stabilize and provide a shell structure to all atoms in the Periodic Table [9]. They are also sufficient to stabilize the H_2^+ and H_2 molecules but overbind them with respect to their separate atomic constituents. The terms V_{m1} and V_{m2} are one- and two-electron functions that correct this discrepancy by preventing localization of the electrons at molecular symmetry points just as V_H prevents localization (collapse) to the atomic symmetry point (the nucleus). There is one parameter associated with each of these four terms.

As shown in Fig. 1, we denote the negative projectile by subscript a, the nuclei of the diatomic target by subscripts b and c, the electrons by 1 and 2, and the midpoint of the homonuclear molecule by o; in addition, Greek subscripts α or β are used in general definitions to designate any of these. The Hamiltonian describing the collision of the negative projectile with a diatomic target will be presented using the following definitions: the relative distance

$$\mathbf{r}_{\alpha\beta} = \mathbf{r}_\beta - \mathbf{r}_\alpha, \tag{4}$$

the relative momentum

$$\mathbf{p}_{\alpha\beta} = \frac{m_\alpha \mathbf{p}_\beta - m_\beta \mathbf{p}_\alpha}{m_\alpha + m_\beta}, \tag{5}$$

and the reduced mass

$$\mu_{\alpha\beta} = \frac{m_\alpha m_\beta}{m_\alpha + m_\beta}. \tag{6}$$

In these definitions a value of "o" for α or β implies the quasiparticle values,

$$m_o = m_b + m_c, \tag{7}$$

$$\mathbf{r_o} = \frac{1}{2}(\mathbf{r_1} + \mathbf{r_2}), \tag{8}$$

and

$$\mathbf{p_o} = \mathbf{p_1} + \mathbf{p_2}. \tag{9}$$

The spin of electron i (up or down) is designated s_i.

The terms in the effective Hamiltonian are as follows:

$$T = \frac{1}{2m_b}p_b^2 + \frac{1}{2m_e}p_1^2 + \frac{1}{2m_c}p_c^2 + \frac{1}{2m_e}p_2^2 + \frac{1}{2m_a}p_a^2, \tag{10}$$

$$V_{\mathrm{Coul}} = -\frac{e^2}{r_{b1}} + \frac{e^2}{r_{bc}} - \frac{e^2}{r_{c1}} - \frac{e^2}{r_{b2}} - \frac{e^2}{r_{c2}} + \frac{e^2}{r_{12}}$$
$$- \frac{e^2}{r_{ba}} - \frac{e^2}{r_{ca}} + \frac{e^2}{r_{a1}} + \frac{e^2}{r_{a2}}, \tag{11}$$

$$V_H = \frac{1}{\mu_{b1}r_{b1}^2}f(r_{b1}p_{b1};\xi_H) + \frac{1}{\mu_{c1}r_{c1}^2}f(r_{c1}p_{c1};\xi_H)$$
$$+ \frac{1}{\mu_{b2}r_{b2}^2}f(r_{b2}p_{b2};\xi_H) + \frac{1}{\mu_{c2}r_{c2}^2}f(r_{c2}p_{c2};\xi_H)$$
$$+ \frac{1}{\mu_{ba}r_{ba}^2}f(r_{ba}p_{ba};\xi_H) + \frac{1}{\mu_{ca}r_{ca}^2}f(r_{ca}p_{ca};\xi_H), \tag{12}$$

$$V_P = \frac{1}{\mu_{12}r_{12}^2}f(r_{12}p_{12};\xi_P)\delta_{s_1,s_2}, \tag{13}$$

$$V_{m1} = \frac{1}{\mu_{o1}r_{bc}^2}f(r_{o1}p_{o1};\xi_{m1}) + \frac{1}{\mu_{o2}r_{bc}^2}f(r_{o2}p_{o2};\xi_{m1})$$
$$+ \frac{1}{\mu_{oa}r_{bc}^2}f(r_{oa}p_{oa};\xi_{m1}), \tag{14}$$

and

$$V_{m2} = \frac{1}{\mu_{12}r_{bc}^2}f(r_{12}p_{12};\xi_{m2}). \tag{15}$$

Following KW we use the form of the constraining function

$$f(rp;\xi) \equiv \frac{(\xi\hbar)^2}{4\alpha}\exp\left\{\alpha\left[1 - \left(\frac{rp}{\xi\hbar}\right)^4\right]\right\}, \tag{16}$$

where ξ is one of the four parameters, $\xi_H = 0.9428$, $\xi_P = 2.609$, $\xi_{m1} = 0.90$, and $\xi_{m2} = 1.73$, and $\alpha = 4.0$ is a constant whose precise value is unimportant but slightly affects the ξ values. The values of ξ_H, ξ_P, ξ_{m1}, and ξ_{m2} are chosen to match the binding energy of the hydrogen atom, the Fermi energy of an electron gas, the dissociation energy of H_2^+, and the dissociation energy of H_2, respectively. Note that $f(rp;\xi) \to 0$ as $\xi \to 0$, thus going over to the purely classical treatment.

The term V_P vanishes in the present application since the two electrons have opposite spins. For the four systems under consideration, $\bar{p} + H_2$, $\bar{p} + D_2$, $\mu^- + H_2$, and $\mu^- + D_2$, the kinetic energy terms are obviously different. The Coulomb terms are identical and the constraint terms are effectively similar. While it is true that the last two terms in V_H and the last term in V_{m1} have coefficients for the $\bar{p}$ and μ^- collisions that are quite different from each other, it is found that capture occurs in highly excited orbitals having large $r_{ba}p_{ba}$, $r_{ca}p_{ca}$, and $r_{oa}p_{oa}$, so these terms have little effect. Thus the differences in cross sections found must be ascribed mainly to the effects of the kinetic-energy terms.

B. Differential equations and trajectories

Hamilton's classical equations of motion are solved with the effective Hamiltonian (1) in the laboratory frame, $\mathbf{r} = \{\mathbf{r}_a, \mathbf{r}_b, \mathbf{r}_c, \mathbf{r}_1, \mathbf{r}_2\}$ and $\mathbf{p} = \{\mathbf{p}_a, \mathbf{p}_b, \mathbf{p}_c, \mathbf{p}_1, \mathbf{p}_2\}$. The 30 coupled equations are

$$\dot{\mathbf{r}} = \nabla_{\mathbf{p}} H_{KWC}, \tag{17a}$$

$$\dot{\mathbf{p}} = -\nabla_{\mathbf{r}} H_{KWC}, \tag{17b}$$

with the chain rule relating the variables of the various potentials to the independent variables of the differential equations. Accuracy of the numerical integration is checked by conservation of energy and angular momentum.

A sufficient number of trajectories, with initial conditions chosen by Monte Carlo, are run to achieve needed precision. The target center of mass is placed at the origin, and the projectile is started at $x = -10a_0$ (except at the lowest energy where $x = -20a_0$ is used) with impact parameter $y = b$ chosen by uniform sampling of $b^2 \in [(b_{i-1})^2, (b_i)^2]$. In the first range $[b_0, b_1]$, $b_0 = 0$ and b_1 is taken to be such that a few ranges of impact parameters will be required to converge the cross sections with $b_{i+1} = \sqrt{2}b_i$. The target is oriented by a random Euler rotation of the KWC representation of the hydrogen molecule, which is given by the coordinates and momenta that minimize the KWC Hamiltonian of the molecule. To within an arbitrary rigid-body rotation, these values in Cartesian coordinates are[1]
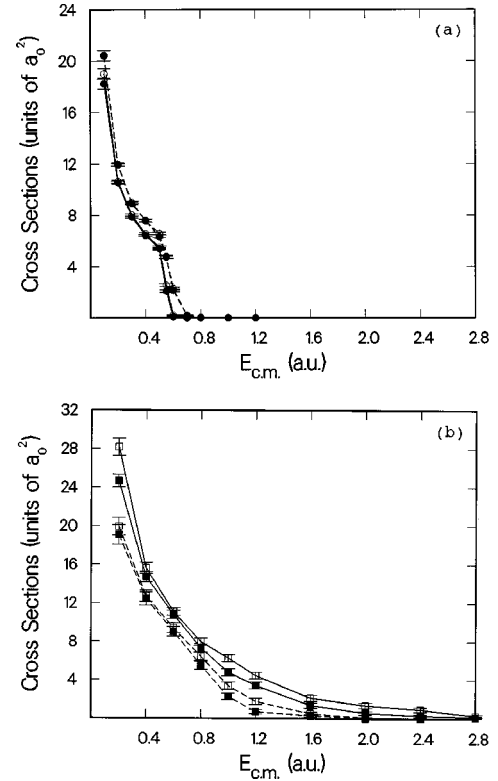

FIG. 2. Capture cross sections for $\bar{p}$ (full curves) and μ^- (dashed curves) collisions with (a) H (open circles) and D (solid circles) atoms and (b) H_2 (open squares) and D_2 (solid squares) molecules.

$$\mathbf{r}_a^{(0)} = -\mathbf{r}_b^{(0)} = (0,0,0.6955),$$

$$\mathbf{r}_1^{(0)} = -\mathbf{r}_2^{(0)} = (0.8714,0,0.3283), \tag{18}$$

$$\mathbf{p}_a^{(0)} = -\mathbf{p}_b^{(0)} = (0,0,0),$$

$$\mathbf{p}_1^{(0)} = -\mathbf{p}_2^{(0)} = (1.0331,0,0),$$

for the parameters given in Sec. II A.

In the quasiclassical description, each particle has definite position and momentum at any given time in its trajectory. The integration is checked every 2000 steps to see if the final state, including the energy and angular momentum of bound states, can be reliably identified. Tentative particle arrangements are identified by interparticle distances, but the conclusive assignments are made by comparing internal energies of the pair or complex with its remaining external interaction potentials. For the current problem, it is important to note that capture of the heavy negative particle $\bar{p}$ or μ^- occurs in a highly excited state. At the instant of apparent capture, the $\bar{p}$ or μ^- usually resides in a complex containing three or more particles. This complex may be short- or long-lived but usually decays into a two-body exotic system, e.g., $p\bar{p}$ or $p\mu^-$. In most cases, it is possible to follow the trajectory long enough to see this final product, which is the main subject of interest. In rare cases the result appears to be a bound three-body system, like $p\bar{p}e^-$ or $p\mu^- e^-$, which can be bound in FMD but not quantum mechanically [10]. Metastable states, like that seen experimentally for $\alpha\bar{p}e^-$ [11–14], could exist, but we make no attempt to analyze them in

TABLE I. Cross sections ($\sigma_{\bar{p}d}$ and σ_{tot}), parameters for fits of n distributions (peak n_0 and half width γ), and parameters for fits of l distributions (rise b, fall a, and cutoff l_1 modify $2l+1$ statistical distribution) for formation of $\bar{p}d$ atoms in (a) $\bar{p}+\text{D}$ and (b) $\bar{p}+\text{D}_2$ collisions. See Appendixes A and B of paper I [1] for formulation of the n and l fits. [Note the following errata: in Eq. (A4), δ should be γ; in Eq. (A15), c should be c_1 on the first line and c_2 on the second line]. There were not enough trajectories forming the exotic atom at the higher energies to allow reliable fits of the quantum-number distributions. Numbers in square brackets denote powers of 10.

$E_{\text{c.m.}}$ (a.u.)	$\sigma_{\bar{p}d}$ (units of a_0^2)	σ_{tot} (units of a_0^2)	n_0	γ	b	a	l_1
		(a) $\bar{p}+\text{D}$					
0.10	18.24 ± 0.43	18.24 ± 0.43	37.44	1.25	$3.23[-03]$	$3.00[-03]$	39
0.20	10.55 ± 0.11	10.55 ± 0.11	42.59	1.80	$1.28[-02]$	$1.95[-02]$	45
0.30	7.87 ± 0.09	7.87 ± 0.09	50.45	3.34	$1.49[-02]$	$4.97[-02]$	51
0.40	6.44 ± 0.08	6.44 ± 0.08	65.66	6.78	$1.44[-02]$	$5.75[-02]$	54
0.50	5.41 ± 0.10	5.47 ± 0.10	108.96	26.08	$8.40[-03]$	$4.62[-02]$	56
0.55	2.11 ± 0.10	5.24 ± 0.15	174.53	53.93	$2.06[-02]$	$1.94[-01]$	58
0.60	0.08 ± 0.02	4.85 ± 0.11					
		(b) $\bar{p}+\text{D}_2$					
0.01	173.04 ± 8.52	173.04 ± 8.52	28.65	1.37	$-4.79[-04]$	$1.73[-01]$	28
0.10	40.15 ± 1.45	40.15 ± 1.45	29.15	2.13	$-2.27[-03]$	$1.61[-04]$	31
0.20	24.31 ± 0.64	25.02 ± 0.70	29.55	3.62	$-2.42[-03]$	$9.97[-04]$	34
0.40	14.63 ± 0.51	18.73 ± 0.82	30.26	4.68	$-2.15[-03]$	$4.61[-05]$	41
0.60	10.81 ± 0.42	16.40 ± 0.77	31.18	4.75	$-1.25[-03]$	$2.35[-08]$	56
0.80	7.25 ± 0.41	13.64 ± 0.71	32.22	4.67	$-2.26[-04]$	$1.18[-01]$	58
1.00	4.78 ± 0.38	12.30 ± 0.73	33.62	5.56	$7.91[-04]$	$4.23[-01]$	60
1.20	3.36 ± 0.36	11.94 ± 0.73	36.79	9.39	$2.50[-03]$	$1.11[+00]$	62
1.60	1.36 ± 0.28	10.39 ± 0.68					
2.00	0.57 ± 0.19	9.89 ± 0.66					
2.40	0.28 ± 0.14	8.98 ± 0.65					
2.80	0.14 ± 0.10	8.83 ± 0.65					

this work. Our procedure also identifies the nonexotic products of the reaction — H_2^+, H, H^-, and H^+.

In the ith range of impact parameter, the contribution to the cross section for a reaction R is given by

$$\sigma_R^{(i)} = \frac{N_i^{(R)}}{N_i^{\text{tot}}} \pi[(b_i)^2 - (b_{i-1})^2] \qquad (19)$$

with standard statistical error

$$\Delta\sigma_R^{(i)} = \sigma_R^{(i)} \left(\frac{N_i^{\text{tot}} - N_i^{(R)}}{N_i^{\text{tot}} N_i^{(R)}} \right)^{1/2}, \qquad (20)$$

where $N_i^{(R)}$ is the number of trajectories in which R occurred out of the total N_i^{tot} trajectories run with $b \in [b_{i-1}, b_i]$. The integrated cross section is thus

$$\sigma_R = \sum_i \sigma_R^{(i)} \qquad (21)$$

with estimated error

$$\Delta\sigma_R = \left(\sum_i (\Delta\sigma_R^{(i)})^2 \right)^{1/2}. \qquad (22)$$

In most cases, 100 trajectories were run in each range of impact parameters, with $b_1 = 1.5a_0$. An exception, where higher precision was needed, is the calculation of laboratory-frame angular-deflection distributions.

III. RESULTS

In paper I, results were presented for $\bar{p}$ capture by the H_2 molecule. In that work emphasis was placed on the difference between capture by the molecule and capture by the atom. In the present work emphasis is placed on differences due to masses, either that of the projectile, $\bar{p}$ or μ^-, or that of the target, H_2 or D_2. The procedures used to fit the quantum-number distributions and the procedures used to artificially constrain molecular motions to test their effects are the same as in paper I; the reader is referred to the Appendixes of that paper for details.

The cross sections for $\bar{p}$ and μ^- capture by the atoms and by the molecules are shown in Fig. 2. The $\bar{p}+\text{D}_2$, $\mu^-+\text{H}_2$, and $\mu^-+\text{D}_2$ cross sections and their statistical uncertainties are given in Tables I–III (similar results for $\bar{p}+\text{H}_2$ were tabled in paper I[2]). The isotope effect for the H and D atomic targets [Fig. 2(a)] can be seen to almost vanish (the differences are within the statistical error bars). Likewise the difference between $\bar{p}$ and μ^- capture by the atom is

_____

[2]Recalculation of the cross section for $\bar{p}+\text{H}_2$ at $E_{\text{c.m.}}=0.01$ a.u. with starting distance $20a_0$ (instead of $10a_0$) showed that the converged value is $169.22\pm8.92a_0^2$ instead of $148.32\pm10.97a_0^2$.

TABLE II. Cross sections ($\sigma_{p\mu}$ and σ_{tot}), parameters for fits of n distributions (n_0 and γ), and parameters for fits of l distributions (b, a, and l_1) for formation of $p\mu^-$ atoms in (a) $\mu^- + H$ and (b) $\mu^- + H_2$ collisions.

$E_{c.m.}$ (a.u.)	$\sigma_{p\mu}$ (units of a_0^2)	σ_{tot} (units of a_0^2)	n_0	γ	b	a	l_1
		(a) $\mu^- + H$					
0.03	54.99±0.43	54.99±0.43	13.19	0.81	5.34[−02]	3.18[−03]	14
0.10	20.41±0.40	20.41±0.40	14.12	0.92	5.66[−02]	1.86[−02]	16
0.20	11.97±0.12	11.97±0.12	15.90	1.24	6.33[−02]	3.15[−02]	18
0.30	9.00±0.11	9.00±0.11	18.47	2.15	6.35[−02]	9.57[−02]	21
0.40	7.60±0.10	7.60±0.10	23.14	4.12	8.27[−02]	2.80[−01]	25
0.50	6.59±0.11	6.67±0.11	31.31	8.33	8.89[−02]	3.57[−01]	27
0.55	4.79±0.12	6.38±0.15	39.58	14.63	9.20[−02]	5.56[−01]	29
0.60	2.29±0.10	6.04±0.16	42.21	18.27	9.89[−02]	1.00[+00]	31
0.70	0.18±0.04	5.63±0.12	38.28	6.98	1.05[−01]	3.84[+00]	33
0.80	0.03±0.02	5.32±0.12					
		(b) $\mu^- + H_2$					
0.01	147.80±10.01	147.80±10.01	10.29	1.34	−1.20[−02]	1.86[−02]	11
0.10	32.80±2.01	32.80±2.01	10.10	1.92	−6.69[−03]	4.11[−02]	13
0.20	19.93±0.92	20.14±0.93	10.64	2.14	−4.20[−03]	1.53[−01]	15
0.40	12.72±0.57	14.91±0.72	12.07	2.81	−9.11[−03]	8.40[−02]	17
0.60	9.40±0.51	12.72±0.69	13.23	3.25	−8.95[−03]	2.26[−04]	23
0.80	6.43±0.42	11.38±0.68	15.07	4.24	−2.11[−03]	3.98[−01]	30
1.00	3.39±0.38	11.03±0.77	17.64	4.15	2.79[−04]	1.07[+00]	36
1.20	1.77±0.32	10.32±0.74	20.67	9.27	−1.11[−03]	6.56[−01]	38
1.60	0.49±0.18	9.68±0.67					
2.00	0.07±0.07	9.68±0.66					

TABLE III. Cross sections ($\sigma_{d\mu}$ and σ_{tot}), parameters for fits of n distributions (n_0 and γ), and parameters for fits of l distributions (b, a, and l_1) for formation of $d\mu^-$ atoms in (a) $\mu^- + D$ and (b) $\mu^- + D_2$ collisions.

$E_{c.m.}$ (a.u.)	$\sigma_{d\mu}$ (units of a_0^2)	σ_{tot} (units of a_0^2)	n_0	γ	b	a	l_1
		(a) $\mu^- + D$					
0.10	20.44±0.40	20.44±0.40	14.53	0.93	5.94[−02]	1.11[−02]	16
0.20	11.93±0.11	11.93±0.11	16.28	1.30	5.76[−02]	2.15[−02]	18
0.30	8.92±0.11	8.92±0.11	18.94	2.09	6.25[−02]	7.29[−02]	21
0.40	7.59±0.10	7.59±0.10	23.74	4.24	1.13[−01]	6.02[−01]	28
0.50	6.35±0.10	6.41±0.11	32.21	8.99	7.84[−02]	5.94[−01]	30
0.55	4.73±0.11	6.21±0.15	39.26	12.49	1.12[−01]	1.02[+00]	32
0.60	2.16±0.10	5.96±0.16	43.77	15.63	1.19[−01]	1.62[+00]	34
0.70	0.18±0.04	5.68±0.12	37.30	3.88	2.59[−01]	5.76[+00]	36
0.80	0.04±0.02	5.39±0.12					
		(b) $\mu^- + D_2$					
0.01	136.83±10.57	136.83±10.57	9.70	1.91	−6.15[−03]	7.33[−02]	12
0.10	30.25±2.17	31.38±2.24	9.54	1.77	1.85[−02]	6.07[−01]	14
0.20	18.73±1.00	19.37±1.03	10.64	2.26	−4.01[−04]	2.66[−01]	16
0.40	12.30±0.67	13.85±0.75	12.32	3.02	−4.34[−03]	1.16[−01]	18
0.60	9.05±0.50	11.31±0.63	14.47	4.24	−8.58[−03]	3.88[−06]	23
0.80	5.44±0.44	10.67±0.74	16.29	5.07	−2.94[−03]	9.45[−04]	26
1.00	2.26±0.33	9.97±0.74	21.14	8.37	−3.71[−03]	2.07[−03]	28
1.20	0.71±0.21	9.47±0.70					
1.60	0.28±0.14	9.05±0.67					

small — the μ^- cross section is slightly larger because the lighter particle behaves less adiabatically. All the atomic cross sections fall off rapidly at energies exceeding the target ionization potential (0.5 a.u.), above which the electron must carry off kinetic energy for capture to occur; i.e., ejection of energetic electrons requires nonadiabatic behavior.

On the other hand, the results for the molecular targets [Fig. 2(b)] are quite different from each other, especially at energies above the ionization potential (0.57 a.u. for the molecule). The cross sections increase in the same order that the mass ratio between the projectile and target nucleus increases, from the smallest for $\mu^- + D_2$ ($m_\mu/m_d = 0.056$) to $\mu^- + H_2$ ($m_\mu/m_p = 0.113$) to $\bar{p} + D_2$ ($m_{\bar{p}}/m_d = 0.50$) to the largest for $\bar{p} + H_2$ ($m_{\bar{p}}/m_p = 1.00$). But even for the poorest match, $\mu^- + D_2$, the cross section is much larger than in the analogous atomic collision $\mu^- + D$. Still at the low energy of 0.1 a.u. the $\bar{p}$ capture is larger than μ^- capture, indicating that the favorable molecular effect is more important than the nonadiabatic effect noted in the atomic case. However, it appears, from the trends of the calculated values, that at extremely low energies, $\lesssim 0.01$ a.u., the μ^- cross section may overtake the $\bar{p}$ cross section.

In order to gain insight into how the molecular cross sections are so dramatically enhanced over the corresponding atomic cross sections, we have done calculations where the molecular degrees of freedom are successively frozen artificially. In the first step we eliminate molecular vibration (and dissociation), treating the molecular target as a rigid rotor; this is accomplished with a Lagrange multiplier λ_{rr} writing the Hamiltonian as

$$H' = H_{KWC} - \lambda_{rr}(r_{bc} - R), \qquad (23)$$

with $R = 1.4a_0$, and adding the equation

$$\partial H'/\partial\lambda_{rr} = 0 \qquad (24)$$

to the set (17). The mathematical details are given in Appendix C of paper I. In the next step, rotations as well as vibrations are eliminated, treating the molecule as a rigid nonrotor; this is similarly accomplished with a vector Lagrange multiplier $\boldsymbol{\lambda}_{rnr}$, writing the Hamiltonian as

$$H' = H_{KWC} - \boldsymbol{\lambda}_{rnr} \cdot (\mathbf{r}_c - \mathbf{r}_b - \mathbf{R}) \qquad (25)$$

and adding the three equations

$$\boldsymbol{\nabla}_{\boldsymbol{\lambda}_{rnr}} H' = \mathbf{0} \qquad (26)$$

to the set (17), as described in Appendix D of paper I. Note that the molecule can still recoil as it should, but the kinematics is determined solely by the molecular center of mass. At this stage only electronic excitation (and ionization) is possible, but the charge distribution is nonspherical, unlike the hydrogen *atom*.

The results of this progression from molecule to atom are shown in Figs. 3(a) and 3(b) for $\bar{p} + H_2$ and $\mu^- + H_2$, respectively. They clearly demonstrate that it is mainly the vibrational effect that distinguishes the capture of the different mass projectiles. Still the rotational effect is also of some importance. Although the rigid-rotor results for $\bar{p}$ and μ^- capture are almost the same, this really indicates that the
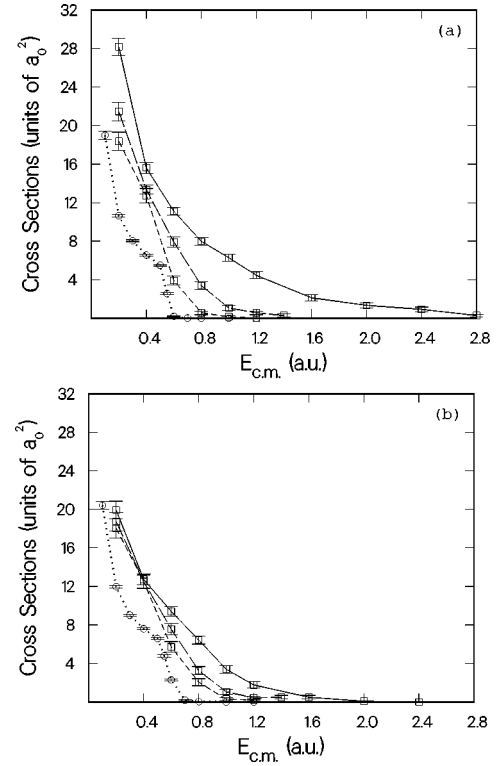

FIG. 3. Comparison of cross sections for (a) $\bar{p}p$ formation and (b) $p\mu^-$ formation: full FMD calculation for H_2 target (full curve), rigid-rotor target (long-dashed curve), rigid-nonrotor target (short-dashed curve), atomic H target (dotted curve).

rotational effect, like the vibrational effect, is greater for $\bar{p}$ than for μ^- since the rigid *nonrotor* results are smaller for $\bar{p}$ than for μ^-. Both of these relationships are as expected from arguments analogous to those above. That is, the mass matching condition for rotational excitation is basically the same as for vibrational excitation. And the rigid nonrotor just allows for electronic effects, albeit two-center, so its cross sections are larger for μ^- than for $\bar{p}$ just as in the atomic case, as expected. Finally we observe that even the nonrotating, nonvibrating molecule has a cross section somewhat greater than that of the atom. At $E \approx 0.5$ a.u. this increase can be attributed in part to the molecule's greater ionization potential; the remainder must be attributed to the two-center charge distribution.

We now consider the quantum numbers of the captured $\bar{p}$ or μ^-. The quasiclassical principal ''quantum'' number n is assigned by the relation

$$n_{qc} = (\mu_{ab}/2E_{bind})^{1/2}, \qquad (27)$$

where E_{bind} is the two-body binding energy of the $\bar{p}$ or μ^- (particle **a**) to the nucleus (taken to be particle **b** here). For capture of heavy negative particles, we obtain $n_{qc} \gg 1$, and thus quite adequate assignments of quantum numbers are given by

$$n = [n_{qc} + 0.5] \qquad (28a)$$

and

$$l = [l_{qc}], \qquad (28b)$$

TABLE IV. *Median* capture energies $\bar{E}_{capt}$ in the unmixed gases and the relative capture probabilities $P_{capt}^{(i)}$ in a mixture of H_2 (fraction c_1) and D_2 (fraction c_2), $c_1 + c_2 = 1$. To a good approximation, $P_{capt}^{(1)}/P_{capt}^{(2)} = qc_1/c_2$, where q is independent of c_i and equal to 1.585 for $\bar{p} + H_2/D_2$ and to 1.186 for $\mu^- + H_2/D_2$.

	$\bar{E}_{capt}^{c.m.}$ (a.u.)	$\bar{E}_{capt}^{lab}$ (eV)	$P_{capt}^{(i)}(c_1=c_2)$
		$\bar{p}$ capture	
H_2	0.610	24.9	0.61
D_2	0.534	18.2	0.39
		μ^- capture	
H_2	0.456	13.1	0.54
D_2	0.432	12.1	0.46

where the brackets designate the greatest integer function.

Rigorous calculation of the distributions of the captured $\bar{p}$ and μ^- *in dense media* would require a complete treatment of the slowing-down kinetics as well as the capture cross sections [15,6]. The slowing-down cross sections have not been calculated in the present work at energies much higher than where capture occurs. However, the slowing down is expected to occur mostly by the same mechanism as capture, namely ionization and dissociation, and thus the energy steps in the slowing down are expected to be similar to the energies where capture occurs. This being the case, the arrival function $F_{arr}(E)$, which is the probability of the free $\bar{p}$ or μ^- having energy E at some time in its history before capture, will be flat. A flat arrival function allows calculation of capture distributions as quadratures over the capture cross sections, e.g., in the case of principal quantum number n,

$$P_n(n) \approx N_n \int_0^\infty F_n(n;E) \frac{\sigma_{capt}(E)}{\sigma_{tot}(E)} dE, \qquad (29)$$

where $F_n(n;E)$ is the distribution calculated for incident energy E and N_n is a normalization constant such that $\sum_{n=1}^\infty P_n(n) = 1$.[3] The probability that the particle is captured before it is slowed to energy E is given by

$$P_{capt}(E) \approx N \int_E^\infty \frac{\sigma_{capt}(E')}{\sigma_{tot}(E')} dE', \qquad (30)$$

where N is such that $P_{capt}(0) = 1$. The median capture energies, where $P_{capt}(\bar{E}_{capt}) = 0.5$, are given in Table IV. This energy is largest for $\bar{p} + H_2$, which has the best projectile-target nucleus mass match, and smallest for $\mu^- + D_2$.

The calculated n and l distributions are shown in Figs. 4(a) and 4(b), respectively, for capture of antiprotons. The analogous distributions for capture of negative muons are shown in Figs. 5(a) and 5(b). Let us first examine the n distributions. The peaks for the distributions coming from capture by the *atomic* targets occur precisely at $n = (\mu_{ab}/m_e)^{1/2}$, which is the exotic orbital that has maximal

---

[3]The *subscript* "n" here is part of the function name, not a variable. In $F_n(n;E)$, the n before the semicolon is the variable of the distribution determined for a given value of the parameter E.
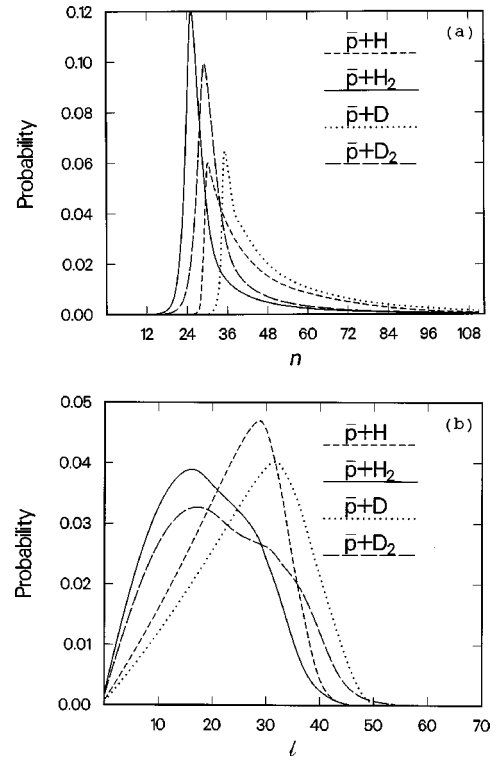

FIG. 4. (a) Principal quantum number n distributions and (b) angular-momentum quantum number l distributions for $\bar{p}$ capture by hydrogen and deuterium atoms and molecules.

overlap with the electronic ground-state orbital as well as binding energy equal to that of the original bound electron. The distributions cut off rapidly on the low-n side since lower n requires the electron to carry off the additional bind-
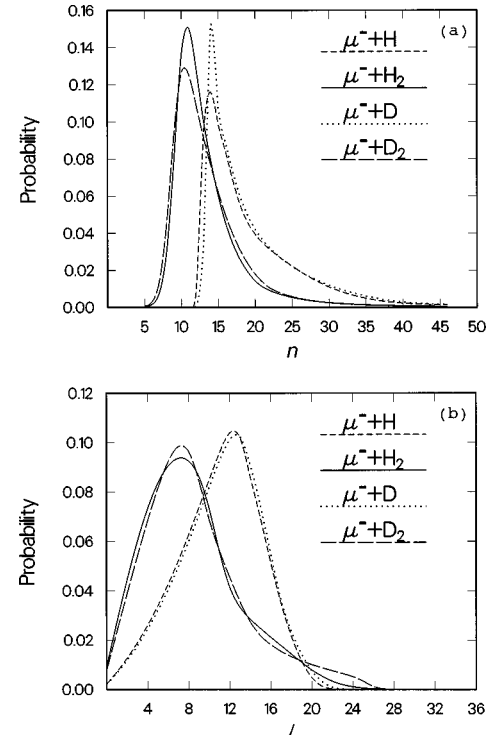

FIG. 5. (a) Principal quantum number n distributions and (b) angular-momentum quantum number l distributions for μ^- capture by hydrogen and deuterium atoms and molecules.

ing energy as kinetic energy and this is unlikely in the essentially adiabatic collisions at very low energies. At high n the distributions fall off as $\sim 1/n^3$, which corresponds to a uniform-energy population of the levels whose energies go as $\sim -1/n^2$.

The n distributions coming from capture by the molecular targets are not so simple. The peaks still depend on the reduced mass, but are shifted to lower n. This shift is partially due to the greater ionization potential of the molecule, which can account for a reduction by a factor of about $(\mathrm{IP_{mol}}/\mathrm{IP_{atom}})^{1/2} = 1.065$, but is due in larger part to the dissociation dynamics, which occurs in the breakup of the intermediate complex. The latter effect depends on the energies carried off by the other particles and cannot be characterized by anything as simple as a multiplicative factor. It can be noted that the energy removed in breakup of the muonic complex is a bit greater than for the antiprotonic complex; this difference is as expected from the less-adiabatic behavior of the muonic system. The tails of the n distributions are also greatly diminished by the energy removed in the breakup of the complex.

Now we turn to the l distributions shown in parts (b) of Figs. 4 and 5. For the atomic targets the distributions are fairly statistical (i.e., proportional to $2l+1$) up to some peak. It has been shown that the peak and maximum l populated are qualitatively interpretable in terms of the overlap of the unperturbed orbital of the target electron with the orbital of the captured heavy negative particle [1]. The situation for the molecular targets is quite different due to their two-center structure. The predominant electron density, lying between the nuclei, tends to emphasize impact parameters equal to or less than half the internuclear distance, leading to a broader peak at lower l than with an atomic target. Also, the rotation of the molecule tends to broaden the distribution of angular-momentum states.

The capture distributions in mixtures can be calculated by a generalization of Eq. (30). In a binary mixture, again assuming a flat arrival function, the probability of capture by component i is given by

$$P_{\mathrm{capt}}^{(i)} \approx N \int_0^\infty \frac{c_i \sigma_{\mathrm{capt}}^{(i)}(E_{\mathrm{lab}})}{c_1 \sigma_{\mathrm{tot}}^{(1)}(E_{\mathrm{lab}}) + c_2 \sigma_{\mathrm{tot}}^{(2)}(E_{\mathrm{lab}})} dE_{\mathrm{lab}}, \quad (31)$$

where c_1 and c_2 are the fractions of each species (here H_2 and D_2), $c_1 + c_2 = 1$, and N is a normalization constant such that $P_{\mathrm{capt}}^{(1)} + P_{\mathrm{capt}}^{(2)} = 1$. The relative capture probabilities for $\bar{p}$ and μ^- capture in $H_2 + D_2$ mixtures are given in Table IV.

Beam experiments are planned for $\bar{p}$ capture with a target that will allow detection of the effect of a single collision [3]. These experiments will enable more direct comparison of experiment and theory, without requiring recourse to integrations over energy as in Eqs. (29)–(31). Though the cross sections displayed in the center-of-mass frame are most instructive for exhibiting the interesting dynamical differences, it is helpful for planning these experiments to view the cross sections in the laboratory frame. The cross sections shown in Fig. 6 are the same as in Fig. 2(b) except as a function of laboratory (projectile $\bar{p}$ or μ^-) energy. Capture of $\bar{p}$ at laboratory energies up to ~ 100 eV is predicted.

Prior knowledge of the angular distributions will be useful in designing the experimental detectors [16]. These dis-
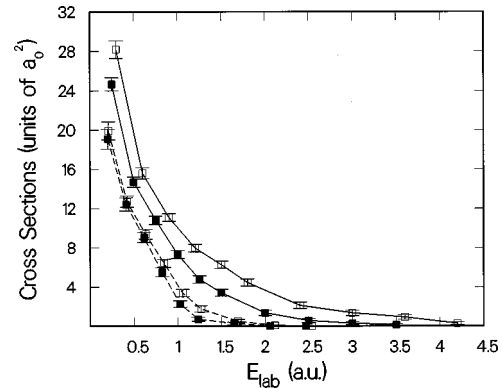

FIG. 6. Capture cross sections in the laboratory frame for $\bar{p}$ (full curves) and μ^- (dashed curves) with H_2 (open squares) and D_2 (solid squares) targets.

tributions are shown in Figs. 7(a) and 7(b) for $\bar{p} + H_2$ and $\bar{p} + D_2$ collisions at a typical collision energy of 0.8 a.u. To obtain suitable statistics for angular distributions, ten times as many trajectories were run at this collision energy. Kinematically all laboratory angles are accessible in $\bar{p}$ collisions with either H_2 or D_2. The dominance at angles less than 90° in the $\bar{p} + H_2$ case shows that the strong collisions are effectively with one nucleus at a time. The distributions are shown separately for three types of outcomes: (i) antiprotonic atoms, (ii) $\bar{p}$ in reactive collisions for which the target is ionized or dissociated, and (iii) $\bar{p}$ in nonreactive collisions for which the target molecule is left intact but may be excited. The antiprotonic atoms are seen to appear at the largest angles with a rather broad flat distribution, mostly in the forward direction for $\bar{p} + H_2$ but extending to the far back-
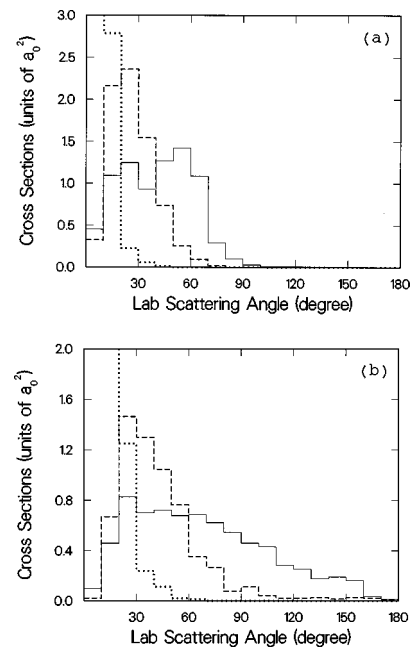

FIG. 7. Histogram of angular distributions of $\bar{p}p/\bar{p}d$ atoms (full curve), free $\bar{p}$ accompanied by *reactive* scattering (dashed curve), and free $\bar{p}$ accompanied by nonreactive (elastic or electronic excitation) scattering (dotted curve) in collisions of $\bar{p}$ with (a) H_2 and (b) D_2 at a c.m. energy of 0.8 a.u. (laboratory energies of 32.6 eV and 27.2 eV, respectively).
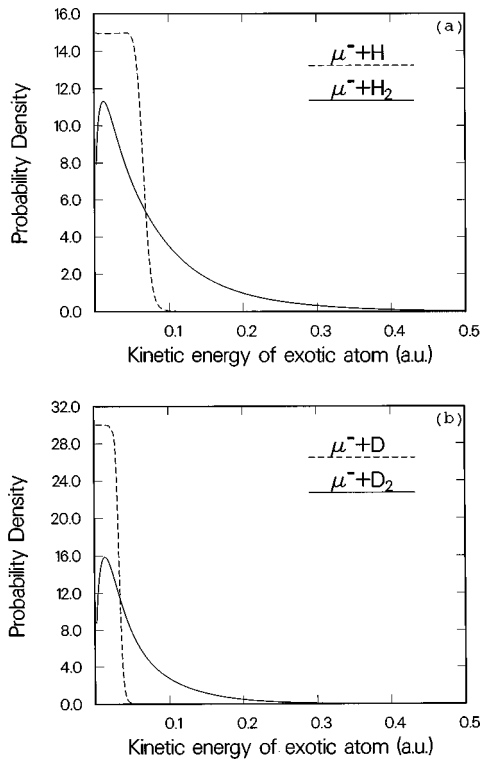
FIG. 8. Kinetic energy distributions of (a) muonic hydrogen $(p\mu^-)$ and (b) muonic deuterium $(d\mu^-)$ atoms formed by muons stopped in dense atomic (dashed curves) and molecular (solid curves) targets.

ward direction for $\bar{p}+D_2$. The transient complex often formed in $\bar{p}+H_2$ and $\bar{p}+D_2$ collisions affects the angular deflections of the exotic atoms formed. The large angles normally resulting from close encounters are further increased by rotation of the intermediate complex before dissociation. The nonreactive scattering is strongly forward peaked since most close collisions result in some particle rearrangement.

Another quantity relevant to interpretation of experiments stopping μ^- in dense targets is the distribution of initial kinetic energies of the exotic atoms formed. The kinetic energy is important in light of recent predictions that the inelastic and muon-transfer cross sections are sensitive to the collision energy and that elastic collisions may not be adequate to thermalize the hot atoms on their time scale [17]. We have calculated the kinetic energy distributions, under assumptions like those leading to Eq. (29), by integrating over the distributions for given incident muon energies E_{lab}. The results are shown in Figs. 8(a) and 8(b) for $p\mu^-$ and $d\mu^-$, respectively. In the case of the *atomic target* the physics is elementary — conservation of linear momentum requires that the kinetic energy of, for example, the $p\mu^-$ atom is just $[m_\mu/(m_p+m_\mu)]E_{\mathrm{lab}}$, *slightly broadened* by the energy of the ejected electron. The interpretation of the kinetic-energy distributions for the *molecular target* is a little more complicated; in this case, the exotic atom is not always emitted in the forward direction *and* the distribution (for a given E_{lab}) is further broadened by the cascade/dissociation dynamics. These effects, as well as the capture cross section which reaches to higher energies in the case of the molecular target, make for significantly higher kinetic energies of exotic atoms formed in collisions with molecular targets. Prac-

tically speaking, only the molecular targets are subject to experiments that slow and capture the μ^- in a dense medium.

IV. CONCLUSIONS

Target molecular structure has been shown to have large effects on capture of both $\bar{p}$ and μ^-. Extant experiments on capture by hydrogen have all been done with molecular targets. Thus most previous theoretical calculations, done for an atomic target, are of dubious relevance. Experiments with target molecules containing different isotopes have been done and more are planned of increasing specificity. In agreement with a recent experiment [18] on stopping antiprotons in H_2+D_2 mixtures, we have found that stopping by H_2 is more probable than stopping by D_2. In fact, our calculations on μ^- as well as $\bar{p}$ capture show a uniform trend: as the mass match between the negative projectile and a nucleus in the target approaches unity, the capture cross sections increase and reach out to higher collision energies. Proposed experiments [3] utilizing a $\bar{p}$ beam of selected energy will provide more stringent tests. We are led to speculate that the relevant match is with the effective nuclear mass, which may be altered by molecular binding [19]. To test this speculation, antiproton experiments with isotopically substituted organic molecules, such as used in past π^- experiments [20], may be useful. In the future, direct experimental comparison of capture by H and H_2 will also be feasible [3,21].

Our test calculations, in which the vibrational and rotational motions of the target molecule were artificially restricted, demonstrate that the vibrational degree of freedom is most important in distinguishing the behavior of the molecule from the atom and in distinguishing different molecular isotopes. However, the effects of rotation, two-center charge distribution, and mass-dependent nonadiabaticity are also significant in determining the cross sections.

The n and l distributions of the exotic atoms formed with molecular targets are found to be quite different from those for atomic targets. In the case of the molecular targets, the maxima of both the n and l distributions are shifted to lower values and the very large n values are suppressed. These quantum-number differences between atomic and molecular targets are largely due to the breakup dynamics of the intermediate complex formed in molecular capture. The quantum-number difference between the two molecular isotopes is mainly a reduced-mass effect, as it is for the different atomic isotopes.

We have calculated the relative initial capture of $\bar{p}$ and μ^- in H_2+D_2 mixtures (Table IV). The initial capture of π^-, of mass $273.14m_e$, can be expected to be similar to μ^-, and experiments exist for capture of π^- in H_2+D_2 mixtures [22,23]. However, the experimental data include the effects of subsequent isotope transfer, which will be quite different for the hadronic π^- (the charge exchange of π^- with the proton provides a distinctive experimental diagnostic as well as the end of its existence). Thus it is not yet possible to compare the present calculations with these experiments. There also exists a very interesting experiment on π^- capture in HD gas [24], which is yet to be fully assimilated with theory. The HD target opens a new possibility in the breakup of the immediate complex — as the π^- evolves from a molecular to an atomic orbital it may go with either the p or d

nucleus. We plan to treat this problem in future calculations. Since *collisional* π^- transfer between isotopes can be expected to be similar in a HD gas and a $H_2 + D_2$ gas mixture, this may enable the desired comparison between theoretical and experimental results.

---

[1] J. S. Cohen, Phys. Rev. A **56**, 3583 (1997), referred to as paper I.

[2] A. S. Wightman, Phys. Rev. **77**, 521 (1950).

[3] T. Azuma *et al.* (ASACUSA collaboration), Atomic Spectroscopy and Collisions Using Slow Antiprotons, experimental proposal CERN SPSC 97-19 (1997).

[4] J. S. Cohen, J. Phys. B **31**, L833 (1998).

[5] N. H. Kwong, J. D. Garcia, and J. S. Cohen, J. Phys. B **22**, L633 (1989).

[6] J. S. Cohen, Phys. Rev. A **27**, 167 (1983).

[7] C. L. Kirschbaum and L. Wilets, Phys. Rev. A **21**, 834 (1980).

[8] L. de Broglie, Philos. Mag. **47**, 446 (1924).

[9] J. S. Cohen, Phys. Rev. A **51**, 266 (1995); **57**, 4964 (1998).

[10] A. M. Frolov and D. M. Bishop, Phys. Rev. A **45**, 6236 (1992).

[11] M. Iwasaki *et al.*, Phys. Rev. Lett. **67**, 1246 (1991).

[12] E. Widmann *et al.*, Phys. Rev. A **51**, 2870 (1995).

[13] R. S. Hayano *et al.*, Phys. Rev. A **55**, R1 (1997).

[14] B. Ketzer *et al.*, Phys. Rev. Lett. **78**, 1671 (1997).

[15] M. Leon, Phys. Rev. A **17**, 2112 (1978).

[16] Y. Yamazaki (private communication).

[17] M. Filipowicz, W. Czapliński, E. Guła, A. Kravtsov, A. Mikhailov, and N. Popov, Nuovo Cimento D **20**, 155 (1998).

[18] A. Bertin *et al.*, Phys. Rev. A **54**, 5441 (1996).

[19] R. G. Sachs and E. Teller, Phys. Rev. **60**, 18 (1941).

[20] D. Horváth *et al.*, Phys. Rev. A **44**, 1725 (1991).

[21] H. Knudsen *et al.*, Phys. Rev. Lett. **74**, 4627 (1995).

[22] V. I. Petrukhin and Yu. D. Prokoshkin, Zh. Éksp. Teor. Fiz. **56**, 501 (1969) [Sov. Phys. JETP **29**, 274 (1969)].

[23] P. Weber *et al.*, Phys. Rev. A **41**, 1 (1990).

[24] K. A. Aniol *et al.*, Phys. Rev. A **28**, 2684 (1983).